Characterization of collector optic material samples exposed to a discharge-produced plasma extreme ultraviolet light source

Darren A. Alman
Huatan Qiu
T. Spila
Keith C. Thompson
Erik L. Antonsen
Brian E. Jurczyk
D. N. Ruzic
University of Illinois at Urbana-Champaign
Urbana, Illinois 61801
E-mail: dalman@starfireindustries.com

Abstract. Extreme ultraviolet (EUV) light sources with efficient emission at 13.5 nm are needed for next-generation lithography. A critical consideration in the development of such a source is the lifetime of collector optics. These experiments expose optics to a large flux of energetic particles coming from the expansion of the pulsed-plasma EUV source to investigate mirror damage due to erosion, layer mixing, and ion implantation. The debris ion spectra are analyzed using a spherical sector energy analyzer (ESA) showing ion energies of 2 to 13 keV, including Xe^{+}-Xe^{+4}, Ar^{+}, W^{+}, Mo^{+}, Fe^{+}, Ni^{+}, and Si^{+}. Microanalysis is performed on samples exposed to 10 million pulses, including atomic force microscopy (AFM), showing increased roughness for most exposed samples. Notably, a Mo–Au Gibbsean segregated alloy showed surface smoothing over this time frame, suggesting that the segregation worked in situ. TRIM predictions for ion implantation are consistent with ion debris measurements from the ESA. Finally, time exposures of samples from 2, 20, and 40 million pulses show an initial roughening with smoothing of the exposed samples at longer time frames. Constant erosion is demonstrated with the SEM. These analyses give an experimental account of the effects of the ion debris field on optic samples exposed to the EUV source.
 [DOI: 10.1117/1.2437212]

Subject terms: extreme ultraviolet lithography; discharge-produced plasma; collector optics; debris; erosion.

Paper 06034R received Jan. 29, 2006; revised manuscript received Sep. 22, 2006; accepted for publication Sep. 27, 2006; published online Feb. 28, 2007.

1 Introduction

Light sources in the extreme ultraviolet (EUV) region are being researched for the high volume manufacturing needs of next-generation lithography. Current lithography uses 193-nm light and can be extended down to the 65- and even 45-nm nodes through various resolution enhancement techniques. Beyond that, however, next-generation lithography methods are needed to meet the advancing expectations of Moore's law by the end of the decade. To meet the economic needs of high volume manufacturing, a wafer throughput of 120 h^{-1} is required, equivalent to 115 W of EUV light from the source.[1] The generated light cannot be focused with lenses due to its absorption by all materials, but is rather collected by reflection off of mirrors. The 13.5-nm wavelength has been chosen because Si/Mo multilayer structures show excellent near-normal reflectivity in the EUV region, with a reflectivity approaching 70% in a narrow bandwidth around 13.5 nm.[2,3] Due to the limitations of the imaging optics in a lithography system, all usable EUV light must come from a region with a maximum etendue of 1 to 3.3 mm^2 sr,[1] translating to a source diameter of <1 mm. Pulsed plasmas with the proper composition and temperature can provide the required output of 13.5-nm light from such a small volume. Two competing methods, discharge-produced plasmas (DPP) and laser-produced plasmas (LPP), are considered candidate technologies.

Mirrors are used to collect the light given off by the plasma over some solid angle and focus it to a spot at the entrance to the illumination optics, called the intermediate focus. Depending on the configuration of the source, mirrors can be positioned to reflect light incident at either normal or grazing angles. At near-normal incidence, multilayer mirrors made of alternating layers of silicon and molybdenum can reflect 13.5-nm light by Bragg reflection due to the different indices of refraction for the two materials. At grazing angles, thicker layers of materials such as molybdenum, ruthenium, or palladium can be used. EUV light is reflected by total internal reflection below a critical angle, with the reflectivity falling off $\propto \theta^{-4}$ above the critical angle.

Both DPP and LPP sources produce strong electric fields during plasma expansion that can accelerate the fuel ions (typically xenon) to extremely high energies on the order of tens of keV. The implication of this is that the mirror surfaces will be bombarded by a potentially large flux of energetic ions, eventually destroying the reflective properties of the mirror. The mechanisms for mirror degradation could be surface erosion, roughening, deposition or implantation of impurities, or layer mixing. The Xtreme Commercial EUV Emission Device (XCEED) at the University of

1537-1646/2007/$25.00 © 2007 SPIE

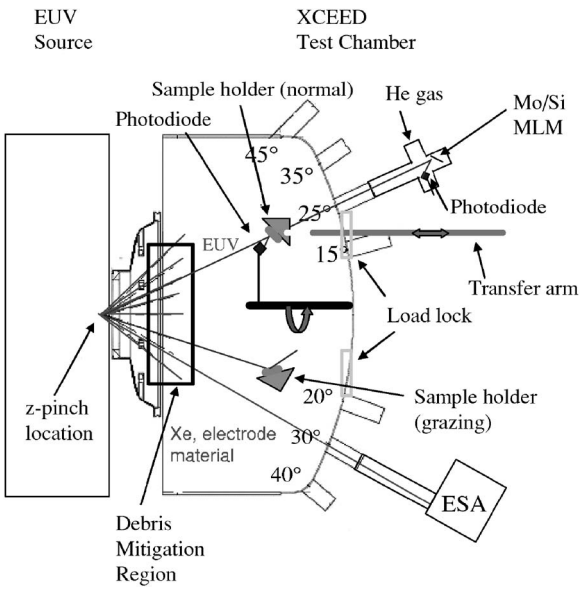

Fig. 1 Diagram of the XCEED experiment.

Illinois[4] has been developed to test the performance of various EUV mirror materials during operation of a commercial EUV source, and to investigate the mechanisms behind any observed losses in reflectivity.

2 Experimental Method

The XCEED experiment combines a commercial EUV source manufactured by Xtreme Technologies GmbH (Gottingen, Germany) with a test chamber. Mirror samples are exposed and debris energies and fluxes can be measured, EUV reflectivity of samples can be measured with a photodiode, and various debris mitigation schemes can be tested in XCEED. The source is an XTS 13–35 z-pinch device, operated with xenon fuel. During exposures, the source runs at 256 Hz and outputs 35 W of EUV light in 2π sr. There is a debris mitigation tool between the source and mirror samples, consisting of a collimating foil trap with some flow of a buffer gas. The samples are mounted on four sample holders that can hold up to sixteen $\frac{1}{2}'' \times \frac{1}{2}''$ square mirror samples each in either a normal incidence or grazing incidence configuration, as shown in the XCEED diagram in Fig. 1. The sample holders can be removed at any time without breaking vacuum through a load lock. This allows groups of samples to be exposed for varying lengths of time and removed independently.

The debris field from the source is measured with a spherical sector energy analyzer (ESA), a well-characterized diagnostic capable of measuring ion energy and discriminating by charge state.[5–7] These experiments use a Comstock model AC-902™ (Oak Ridge, TN) with dual microchannel plate detectors from Burle Industries (model CP-618C™) (Lancaster, PA). The analyzer has line-of-sight access to the source through 2 $\frac{3}{4}$ in. CF half nipples positioned at angular intervals of 5 deg from 15 to 45 deg from the centerline of the pinch. Access at 0 deg is impeded by the beam stop of a debris mitigation tool. Current experiments are performed at 20- and 30-deg angles. Data acquisition for the ESA is triggered by the rising light signal from a photodiode. The ESA is mounted on a bellows connection to the chamber for 3-D pointing control. The entrance orifice to the ESA deflector section is 3 mm in diameter, and total distance traversed by the ions from the source to the microchannel plates is 150 cm. The ion current to the ESA is actually limited by a 1-mm-diam orifice located 97 cm from the pinch, between the pinch and the ESA. Details on the debris field measurements are published elsewhere.[8]

The eight samples investigated consist of one Si/Mo multilayer mirror (MLM), six single material films of thickness 200 nm deposited on silicon substrates, and one alloy film deposited on silicon with a thickness of 20 nm. The multilayer is optimized for 5-deg operation with 50 bilayer pairs with a period thickness of 6.95 nm and a gamma of 0.4, and has a 2.3-nm ruthenium capping layer. The seven single films are carbon, gold, molybdenum, palladium, ruthenium, and silicon. The MLM and single films were prepared by Bajt at Lawrence Livermore National Laboratory.

The alloy sample consists of a molybdenum and gold film deposited simultaneously in an AJA 2000 custom cosputtering tool at the Microfabrication and Crystal Growth Facility at the University of Illinois' Materials Research Laboratory. Molybdenum is chosen to act as a mirror at grazing angles, while gold is chosen for its tendency to segregate to the molybdenum surface and for its ease of sputtering. Gold will accumulate near surfaces due to the difference in potential energies for Mo and Au between bulk material and free surfaces, a process known as Gibbsean segregation.[9] The idea is that gold will continually segregate to the surface and be sacrificially sputtered by debris ions, thereby preserving the reflective molybdenum film.

Two identical sets of the eight samples were used. The first set was not exposed to the EUV light source, but was characterized at the Center for Microanalysis of Materials (CMM) at the University of Illinois. Several different characteristics were measured, including the roughness of the surfaces, the film texture, thickness, and composition. A second set of eight samples were exposed in the XCEED experiment for 10 million shots over approximately 11 h. The gold, carbon, multilayer mirror, molybdenum, and silicon samples were exposed at near-normal incidence (10 deg from normal). The molybdenum-gold alloy, palladium, and ruthenium samples were exposed at grazing (67 deg) incidence. After exposure, the samples were taken to the CMM and characterized using the same procedure that the pre-exposure samples had used.

3 Results

3.1 *Debris Characterization*

Characterization of the z-pinch ejecta in the DPP source is performed with a spherical sector energy analyzer (ESA) to measure fast ion species and their energy spectra. This evaluates the debris mitigation tools ability to divert direct fast ion impact and erosion effects on collector optic surfaces. The debris mitigation tool is a dual foil trap with argon gas curtain.[10] Microanalysis results are compared to the measured direct ion debris field to determine its contribution to total material erosion and the ability of the debris mitigation tool to effect attenuation of fast ion debris. Xe^+

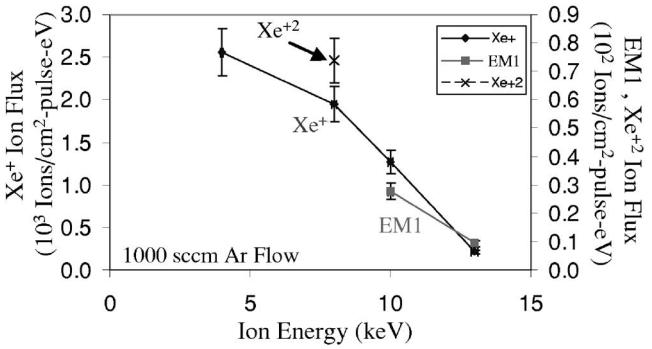

Fig. 2 Debris spectrum measured in XCEED with the TOF-ESA diagnostic at 1000 sccm Ar flow, showing the energy spectra of detected Xe^+, Xe^{2+}, and electrode material 1 (EM1).

up to Xe^{+4} ions are measured along with Ar^+ (buffer gas), electrode materials such as W^+, Mo^+, and Si^+, and finally debris tool materials including Fe^+ and Ni^+. Energy spectra for these species from 0.5 keV up to 13 keV are defined at 20 and 30 deg from the pinch centerline in the DPP chamber. Results show creation of high energy ions and a drop in ion flux with angular increase (Fig. 2).[11] The dominant specie is Xe^+, which peaks around ~8 keV, followed by Xe^{2+}, which maximizes at ~5 keV. Ion flux measured against buffer gas flow rate suggests that the direct fast ion population is significantly attenuated through increases in buffer gas flow rate. Data from sample analysis and ESA measurements indicate mechanism and effect for debris-optic interactions and detail the effectiveness of the current debris mitigation schemes.[12]

3.2 *Mirror Degradation*

The damage to mirrors was analyzed at the Center for Microanalysis of Materials at the University of Illinois. A set of unexposed samples and a set taken out of XCEED were analyzed in an identical manner to accurately gauge the effects that exposure had on several key properties—surface roughness, texture, amount of erosion, and implantation.

3.2.1 *Surface roughness*

The surface roughness of an EUV mirror affects its reflectivity, particularly for a mirror designed to operate at a glancing angle, because of the small wavelength of the EUV photons. For example, roughness on a length scale similar to the wavelength of the photons can alter the actual angle of incidence that the photons make with the surface, reducing the reflected intensity in the expected direction.

Surface roughness is primarily investigated using atomic force microscopy (AFM) on a Digital Instruments Dimension 3100 AFM (Veeco, Woodbury, NY). Scans are performed with 5×5, 2×2, 1×1, and 0.5×0.5-μm scan sizes. The 2×2-μm scans were chosen for the most detailed analysis, to coincide with roughness data taken by the providers of the films. The results are summarized in Table 1. Pre-exposure samples are generally smooth, particularly silicon and carbon where the root mean squared (rms) roughness is calculated to be close to 1 Å. The metals are slightly rougher, ranging from 0.23 nm for the ruthenium capping layer of the multilayer to 1.53 nm for the molybdenum-gold alloy. The average RMS roughness over all samples is 0.47 nm.

After exposure in XCEED, the roughness measurements are repeated in an identical fashion. In general, the roughness of the samples increased by ~2 to 5 times as a result of the 10 million shot exposure. The largest change is seen in carbon, where the rms roughness increased by a factor of 5.4. There are two cases in which roughness did not increase the MLM and Mo-Au samples. In the case of the multilayer mirror, this result could be explained if the ruthenium capping layer is eroded, leaving the intrinsically smoother silicon layer as the top surface. This agrees with the postexposure measurement that shows a 0.13-nm rms roughness of the multilayer mirror, a very low value close to that of unexposed silicon. It is not completely clear why the Mo-Au alloy sample becomes smoother, although the idea behind using the Gibbsean segregated alloy is that the surface will be dynamic during exposure, e.g., molybdenum and gold will be sputtered at different rates from the surface, and gold will constantly diffuse toward the surface. It is possible that this surface replenishment maintains a

Table 1 Surface roughness measurements from AFM and XRR measurements.

		AFM-rms roughness (nm)			XRR-rms roughness (nm)		
Sample	Geometry	Pre-exposure	Post-exposure	Post/Pre	Pre-exposure	Post-exposure	Post/Pre
Au	Normal	0.46	1.55	3.37	1.11	1.79	1.61
C	Normal	0.16	0.86	5.38	0.79	9.2	11.65
MLM	Normal	0.23	0.13	0.57	0.25	0.15	0.60
Mo	Normal	0.33	0.76	2.30	1.7	2	1.18
Mo-Au	Grazing	1.53	0.76	0.50	0.17	0.017	0.10
Pd	Grazing	0.61	1.28	2.10	1.26	1.14	0.90
Ru	Grazing	0.32	0.8	2.50	0.31	0.98	3.16
Si	Normal	0.11	0.26	2.36	—	—	—

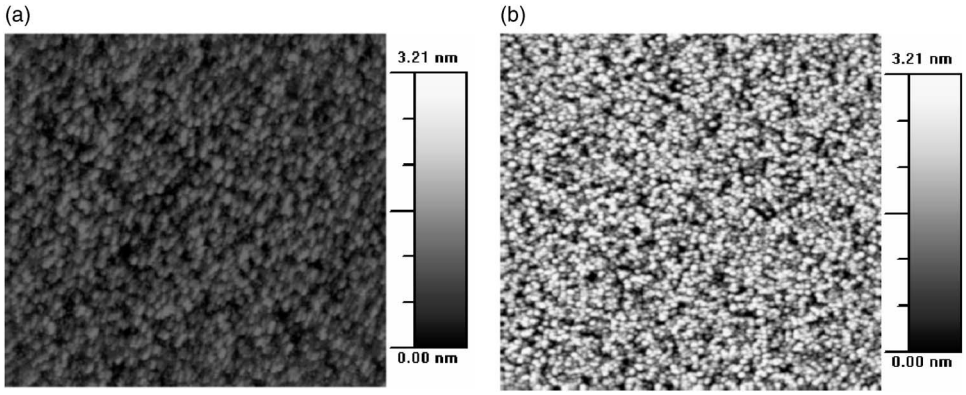

Fig. 3 AFM data for ruthenium (a) before and (b) after exposure for 20 million shots in XCEED. The color scale is the same in both scans, clearly showing the increase in height variations after exposure.

smooth surface. This is something that is currently being studied further. On average, the exposures increase rms roughness by 70%.

The AFM results are checked against x-ray reflectivity (XRR) measurements, performed on a Philips X'pert (Amsterdam, Netherlands. XRR gives an estimate of the surface roughness from the rate at which the reflected intensity falls off beyond the critical angle, i.e., as you move further away from grazing incidence. The Fresnel equation predicts a theoretical decrease in reflectivity proportional to the inverse of the angle to the fourth power for an ideal surface. Surface roughness causes reflectivity to fall off faster than in the ideal case. The roughness values in Table 1 are calculated by fitting a theoretical curve to the XRR data.

The AFM and XRR results agree that on average over all samples, those exposed to the EUV light source are approximately twice as rough as the unexposed samples. The XRR measurements also confirm the two somewhat unexpected results reported earlier, namely that the multilayer and Mo-Au samples are smoother after exposure. The rest of the samples, with the exception of palladium, show an increase in surface roughness after exposure. Because the XRR calculations of surface roughness come from fitting the data to a model, the AFM measurements provide a more direct measurement of roughness and are probably more reliable (Figs. 3 and 4).

3.2.2 *Texture*

The orientation of crystal planes in the material, or its texture, is important for understanding diffusion processes. For example, the metals studied here typically grow as long fibers oriented normal to the surface when deposited on silicon. In this orientation, diffusion would more readily occur along grain boundaries in the direction normal to the surface than in the direction parallel to the surface. The texture can also influence the impurity adsorption and oxidation resistance of the capping layer.[13]

Measurements of the preferred orientation of crystallites, or texture, of the samples are made using x-ray diffraction (XRD). Several different types of scans are performed. A θ–2θ scan uses a symmetrical geometry where the angle between the surface plane and x-ray source (ω) is equal to the angle between the surface plane and the x-ray detector (θ). A scan over a range of angles with ω and θ coupled, while recording the diffracted intensity gives the overall crystallinity of the sample as well as the out-of-plane lattice spacing. The intensity peaks in the out-of-plane lattice spacing show which crystal orientations are present in the sample. The results of the θ–2θ scans are given in Table 2. In all cases, the films are grown on a (100) silicon substrate, so no peaks are seen around the dominant peak from the substrate between 60 and 70 deg. This also makes it impossible to learn much from the silicon film. It is either amorphous or has the same orientation as the silicon substrate. The carbon film and the Mo-Au alloy do not show any peaks in the θ–2θ scan. The Mo-Au alloy is likely too thin to give good data, and the carbon film is possibly amorphous. In the cases that do yield good data, all samples show a strong preference for one orientation, as evidenced by relative peak heights significantly different than would be expected in an untextured sample of the same material. Gold, molybdenum, palladium, and ruthenium favor the (111), (110), (111), and (002) orientations, respectively.

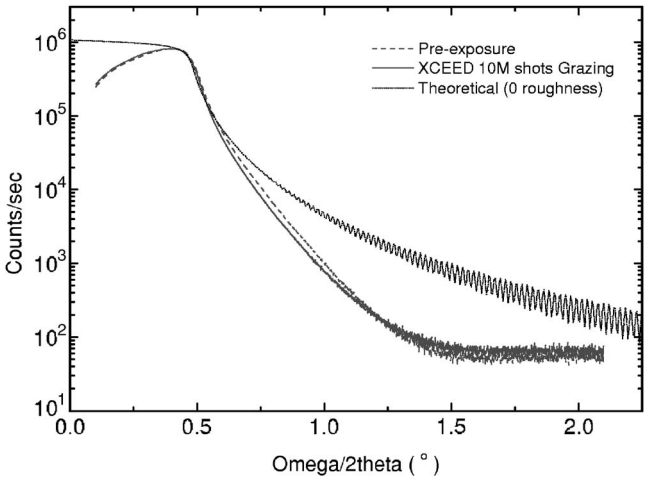

Fig. 4 XRR results for the pre- and postexposed ruthenium film, compared to a theoretical reflectivity for a perfectly smooth ruthenium surface. The film exposed in XCEED exhibits more roughness than the unexposed sample.

Table 2 X-ray diffraction θ–2θ peaks, normalized to the largest peak that would be found in an untextured sample.

			Normalized peak height			FWHM of rocking curve (deg)	
Sample	2θ (deg)	h k l	Untextured	Pre-exposure	Post-exposure	Pre-exposure	Postexposure
Au	38.185	1 1 1	100	100.0	100.0	5.78	5.68
	44.393	2 0 0	52	0.0	0.0	—	—
	77.549	3 1 1	36	0.1	0.2	—	—
	81.724	2 2 2	12	2.4	4.4	—	—
Mo in MLM	40.550	1 1 0	100	100.0	100.0	13.1	13.3
	58.661	2 0 0	16	0.0	0.0	—	—
	73.753	2 1 1	31	0.0	0.0	—	—
	87.687	2 2 0	9	3.3	6.0	—	—
Mo	40.550	1 1 0	100	100.0	100.0	12.3	13.0
	58.661	2 0 0	16	0.7	0.7	—	—
	73.753	2 1 1	31	2.3	4.7	—	—
	87.687	2 2 0	9	1.7	2.9	—	—
Pd	40.119	1 1 1	100	100.0	100.0	8.44	8.44
	46.659	2 0 0	60	0.5	0.7	—	—
	82.100	3 1 1	55	0.5	1.2	—	—
	86.619	2 2 2	15	1.5	2.9	—	—
Ru	38.420	1 0 0	40	29.0	28.0	—	—
	42.189	0 0 2	35	797.0	826.0	9.53	9.63
	44.044	1 0 1	100	100.0	100.0	—	—
	78.465	1 0 3	25	2.0	4.2	—	—
	82.305	2 0 0	6	0.0	0.0	—	—
	84.790	1 1 2	25	2.5	5.5	—	—
	86.046	2 0 1	20	3.7	7.4	—	—

The θ–2θ scan also provides quantitative information on grain size of the films, by fitting a curve to the peaks and applying the Scherrer equation,

$$L = \frac{k\lambda}{B \cos \theta}, \tag{1}$$

where L is the average crystallite size measured normal to the surface of the sample, k is a constant taken to be 0.9, λ is the wavelength of the x-rays, and θ is the Bragg angle. The peak width B comes from the θ–2θ and the contribution of the instrument, in this case

$$B = \sqrt{B_{\text{measured}} - B_{\text{instrument}}} = \sqrt{B^2_{\text{measured}} - (0.17)^2}. \tag{2}$$

The results of these calculations are shown in Table 3. The grain sizes for the metallic films are between 250 and 350 Å. The Mo–Au alloy has smaller grains, under 100 Å in size. After exposure in the DPP EUV light source, the grain sizes mostly decrease slightly—except for the gold sample, which shows a very small increase. Overall, there is not evidence of much modification of grain size through DPP exposure.

A rocking curve can show how strongly orientations are preferred. This is a scan where ω is varied with a fixed 2θ angle. The intensity curve will form a Gaussian peak, with the broadness of the peak giving information on the overall crystallinity of the film. A single crystal has a very narrow peak, because as soon as the ω angle is moved the smallest amount, the condition for reflection is broken. Conversely, for completely random orientations, as ω is varied there are always the same number of crystallites able to reflect the x-rays, resulting in a flat rocking curve. Rocking curves are performed on the dominant peak in each sample's θ to 2θ scan. The results are given in Table 2. The peak widths show little change after exposure in XCEED. In a couple of cases the peaks show slight broadening, indicating that some breakup of the grains occurred, but overall there was little change.

A pole figure is a texture measurement performed by rotating the sample about its surface normal (φ) and tilting the sample about its axis parallel to the direction of the x-rays (ψ). The source (ω) and detector (θ) angles are fixed to look at a particular orientation of planes. Pole figures give the preferred orientation and tell whether the sample is

Table 3 Omega rocking curve and psi scan results for pre- and postexposure samples.

		Grain size from θ–2θ (Å)			Fraction of randomly oriented grains from ψ scan (%)		
Sample	Orientation	Pre-exposure	Postexppsire	Post/Pre	Pre-exposure	Postexposure	Post/Pre
Au	Normal	351	367	1.05	0.11	0.02	0.22
MLM	Normal	—	—	—	15.04	15.24	1.01
Mo	Normal	243	241	0.992	4.41	2.46	0.56
Mo–Au	Grazing	94.7	70.5	0.744	—	—	—
Pd	Grazing	368	352	0.957	2.23	0.71	0.32
Ru	Grazing	324	317	0.978	1.05	0.82	0.79

single or polycrystalline. The pole figures show that the metal films (Au, Mo, Pd, and Ru) exhibit a fiber texture, meaning that there is a preferred lattice plane that points toward the surface of the film. The preferred orientation shows up as a sharp peak at $\psi=0$ deg, as gold's preferred (111) orientation does in the gold (111) pole figure [Fig. 5(a)], and as a ring with a constant intensity at a tilt angle (ψ) of 54 deg as the sample is rotated in φ in gold's (002) pole [Fig. 5(b)]. The tilt angle of the ring is exactly the angle between the (111) and (002) planes. This means that there are many different grains with random rotations in the φ direction. If the sample were a single crystal, the preferred orientation would appear as four discrete peaks separated by 90 deg in φ.

A psi scan (or fiber plot) is done by varying the tilt angle of the sample (ψ), and measuring the change in intensity versus angle. In a film exhibiting a fiber texture, where the preferred lattice plane points toward the surface of the film, the psi scan gives the sharpness of the peak in the pole figure at $\psi=0$ deg with much better resolution than the pole figure achieves. The sharpness of the peak indicates how well oriented to the surface the grains are, e.g., if some grains have a slight tilt with respect to the surface, it will broaden the psi scan. Quantitatively, the ratio of the area under the curve up to the minimum measured intensity to the area under the entire curve gives the fraction of randomly oriented grains in the film. The results of such calculations are summarized in Table 3. The data show that there are generally fewer randomly oriented grains after exposure in the DPP source, with only the multilayer sample remaining unchanged.

3.2.3 *Erosion*

Erosion is of considerable importance when dealing with a multilayer mirror. Erosion will first remove any capping layer present, and then begin to destroy silicon and molybdenum layers underneath. As fewer Si-Mo interfaces are present, the reflectivity would drop accordingly. It is for this reason that the multilayer mirror is deposited with 50 layers originally, so that as layers are eroded there are new ones underneath that can begin to reflect the EUV light.

Sputtering of mirror material by energetic ion impact is potentially a serious problem in an EUV source. The ion fluxes can reach 1.7×10^{14} m^{-2} s^{-1} with ion impact energies up to 13 keV, even with a buffer gas, as measured in XCEED.[8]

The samples are analyzed with scanning electron microscopy (SEM) to look at the cross sectional film thickness before and after exposure in XCEED (Fig. 6). Results are summarized in Table 4, showing that erosion ranges from 10 to 50 nm for the various materials. Several films proved difficult to measure properly. The 200-nm silicon and carbon films on a silicon substrate presented problems because of poor contrast between the film and substrate material. Compositional information comes from detection of backscattered electrons, the intensity of which depends

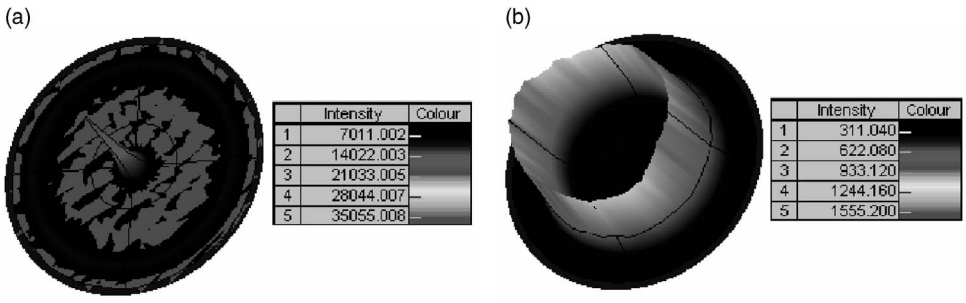

Fig. 5 (a) (111) and (b) (002) pole figures for gold after exposure for 20 million shots in XCEED. There is a strong peak at $\psi=0$ deg in the (002) pole figure that shows up as a ring at $\psi=54$ deg in the (111) pole figure, indicating the gold film has a fiber texture. The pole figures for the pre-exposure samples were nearly identical to those of the exposed samples.

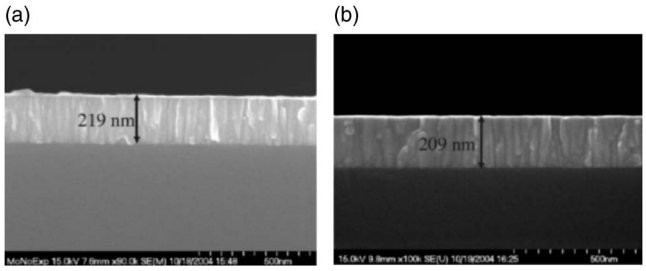

Fig. 6 SEM pictures of the molybdenum film (a) before and (b) after exposure for 20 million shots in XCEED. The film showed a ~10-nm decrease in thickness due to erosion.

on the atomic number. Therefore, the heavier metallic films do not present such a problem. The ruthenium film appears to have delaminated from the substrate and hence is impossible to accurately measure.

While it is theoretically possible to get a thickness estimate from Auger electron spectroscopy (AES) depth profiles by measuring the atomic concentration of the film versus sputtering time, the sputtering rate in the AES instrument varied too much during these measurements to accurately estimate thicknesses.

3.2.4 *Implantation*

As energetic ions bombard the surface, many of them travel some distance into the material before coming to rest. If they remain trapped in the surface, then this can have an effect on material properties such as index of refraction that is critical in the reflection processes. Similarly, layer mixing (e.g., Si and Mo layers mixing together) destroys the sharp transition from one index of refraction to another between the silicon and molybdenum layers needed for a multilayer mirror to function. This can occur as incident ions impart kinetic energy to silicon or molybdenum atoms in the mirror sufficient to displace them from their lattice positions and into adjacent material layers.

Because the debris characterization measurements showed that xenon and the other materials found in the debris spectrum had kinetic energies ranging from 2 keV to at least 13 keV, we expect that these materials will be found implanted into the mirror samples. From Transport of Ions in Matter (TRIM) simulations,[14] the average range of an 8.4 keV Xe^+ ion would be anywhere between 1.9 nm in ruthenium at a grazing angle of 67 deg from normal to 11.4 nm in silicon at 10-deg incidence. The maximum range can be several times the average, e.g., close to 10 nm in ruthenium at 67 deg. To verify this, we looked at the eight samples in AES and x-ray photoelectron spectroscopy (XPS). Both techniques analyze the energy of electrons emitted from very-near-surface electrons, either due to electron (AES) or x-ray (XPS) irradiation. The energy of the emitted electrons is characteristic of the element that they came from, allowing for determination of elemental composition. By simultaneously sputtering the sample, a depth profile of atomic concentration is obtained.

In Auger, we perform depth profiles all the way through the samples until the silicon substrate is reached. However, most of the interesting composition information is expected near the surface, so the sputtering rate is initially set to be rather slow. The XPS instrument does not allow for continuous depth profiling, as was done in AES. However, we scan after six different amounts of sputtering with argon (0, 23, 88, 157, 227, and 296 s) for the multilayer mirror and (0, 40, 80, 120, 160, and 200 s) for seven remaining samples. The sputtering rate is calibrated at ~30 Å of SiO_2 per minute. The sputtering times for the multilayer are chosen to roughly correspond to locations in the middle of the layers.

The results show small amounts of material on the sample surfaces from the vacuum chamber and other samples. The gold, palladium, ruthenium, and molybdenum seen on some samples most likely originate from redeposition of material sputtered from adjacent samples. Iron is also present, and probably originates from steel components inside the vacuum chamber. All of these occur near the surface, but are not seen after sputtering away some of the sample. Figure 7 shows an example of this in the case of the multilayer mirror sample. Pd, N, Sn, O, and Fe are all seen on the surface scan, but their intensities are decreased after sputtering with argon, suggesting that they deposited on the surface with little kinetic energy. Palladium was most likely sputtered from a nearby palladium sample and redeposited on the multilayer.

Table 4 SEM film thickness measurements and erosion calculations.

		Thickness (nm)			
Sample	Geometry	Unexposed	Exposed	Net erosion	Predicted
Au	Normal	219	165	54	33.0
C	Normal	—	—	—	1.1
MLM	Normal	355	342	13	8.5
Mo	Normal	219	209	10	6.5
Mo–Au	Grazing	30	—	—	10.0
Pd	Grazing	278	258	20	18.0
Ru	Grazing	186	200	−14	11.0
Si	Normal	—	174	—	5.8

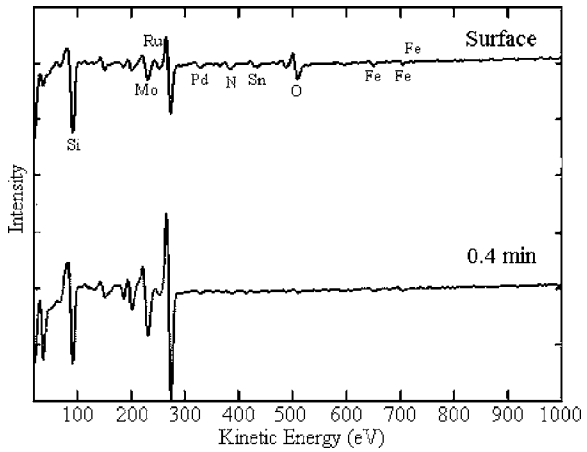

Fig. 7 Auger electron spectroscopy data from the multilayer mirror sample after exposure in XCEED. Surface contaminants Pd, N, Sn, O, and Fe are mostly removed after 0.4 min of sputtering with argon.

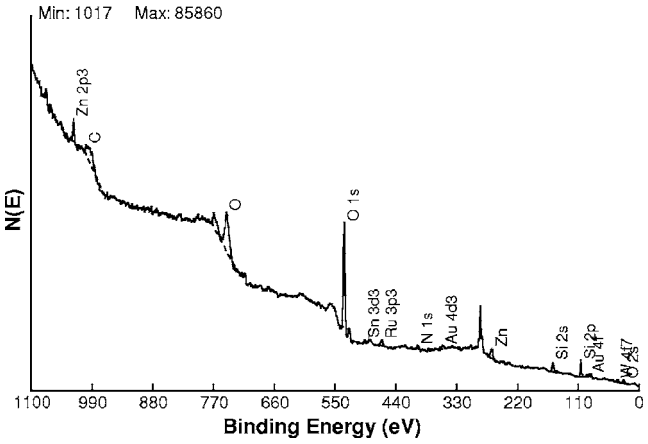

Fig. 8 X-ray photoelectron spectroscopy data for the silicon sample after 200 s of sputtering with argon (a depth of ~8.5 nm). Tungsten is found in the sample at least up to this depth, indicating that it was implanted with a good deal of energy.

Xenon and tungsten are present in at least some of the samples even after 200 s of sputtering with argon, e.g., in the silicon sample as shown in Fig. 8. This would indicate that they were implanted with considerable kinetic energy, qualitatively matching the results of the time-of-flight (TOF)-ESA diagnostic.[8] It is difficult to back out an accurate energy estimate from the XPS data because of uncertainties in the calculating the depth from the sputtering time.

3.3 *Time-Dependent Exposures*

A second set of exposures is done on one material selected from the eight discussed so far, namely the ML1 sample for normal incidence exposure. The Si/Mo multilayer is the obvious choice because such a material will be used for any normal incidence EUV mirrors. This time, four samples of the same material are placed in the XCEED device and exposed for a maximum of 40 million shots. The objective is to expose identical samples to varying exposure lengths and observe the differences in the materials afterward. One sample is to be removed after only 2 million shots, one after 10 million shots, another after 20 million shots, and finally one sample was to remain in the device for the full 40 million shots. However, there is a problem with the transfer arm during the experiment, and as a result two samples were exposed to the full 40 million shots, i.e., there was no sample removed after 20 million shots. The other two were exposed to 2 million and 11 million shots as planned.

Another interesting development during this experiment is that during the 40 million shot exposure, which was performed over the course of two days, the electrodes experienced significant erosion and reached their end of life. The EUV light output, as measured by the in-situ EUV photo-

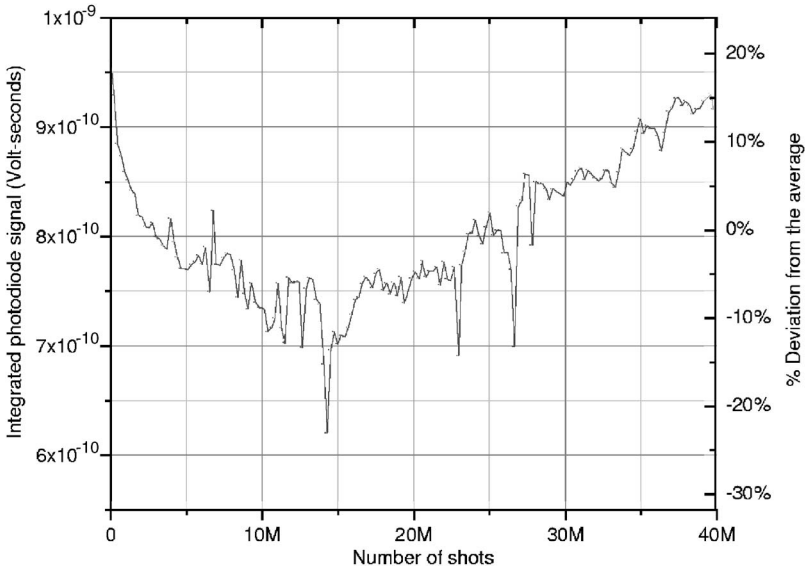

Fig. 9 EUV output during the time-dependent exposures, as measured by the in-situ photodiode.

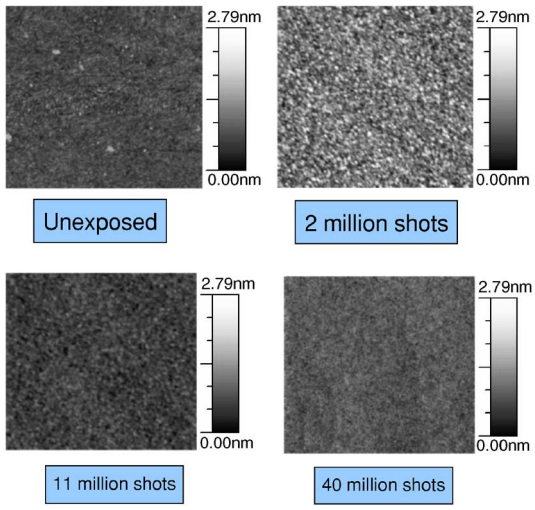

Fig. 10 Surface roughness from AFM scans of samples after 2, 11, and 40 million shots. Roughness first increases and then smoothes back to the unexposed level.

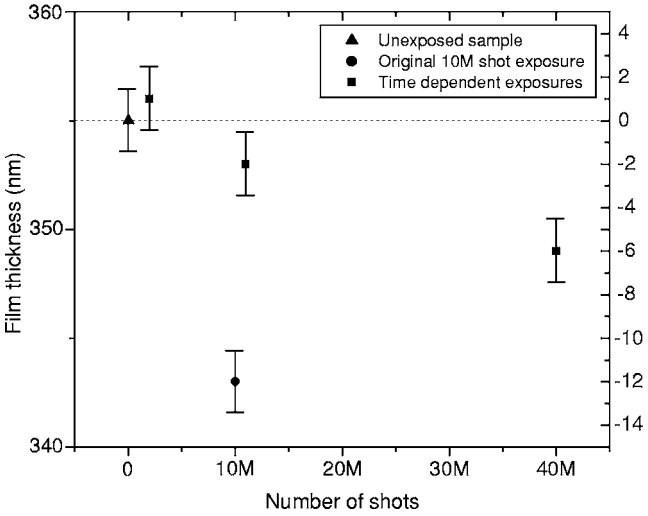

Fig. 11 Measured erosion versus time. At first, the sample gets thicker, which may correlate to the roughness increase that is also seen. Then erosion increases with time.

diode, varies over the course of the exposures as shown in Fig. 9. At the end of the 40 million shots, it was discovered that the electrodes were eroded away and required replacement.

Postexposure analysis of the samples is done in an identical fashion to the first exposures of eight samples. AFM results (shown in Fig. 10) show that after 2 million shots, the sample is rough (0.53-nm rms), compared to unexposed samples that are typically ~0.22 nm). However, after 11 million and 40 million shots, the rms roughness returns to the level of unexposed samples. This indicates an initial roughening of the surface, but over time as they are eroded away, the surfaces regain some smoothness. In addition, the AFM data show that initially the height variations are relatively course after 2 million shots, but over time become gradually finer after 11 million and ultimately 40 million shots. This seems to agree with the smoothing that was observed over time.

Cross sectional views of the films are taken in SEM after the time-dependent exposures, just as in the first exposures. Thickness estimates from SEM photographs show a definite trend toward decreasing film thickness as the exposure time increased—a sign of sample erosion during exposure. However, the slope of the thickness versus time curve (as shown in Fig. 11) seems to be flatter than in previous experiments. This may indicate that during the time-dependent exposures, there was a higher rate of material being deposited on the sample surfaces, e.g., from metal being sputtered or evaporated from the electrodes, which in turn offset to some extent the erosion that was taking place simultaneously.

4 Conclusions

We present an experimental investigation of the effect of plasma exposure on various EUV mirror materials, which is a critical issue for the lifetime of collector optics. Eight different samples were characterized before and after the exposure, and several key properties including surface roughness, texture, erosion, and implantation are reported using various material characterization techniques. A spherical sector energy analyzer (ESA) is used to evaluate the ability of a debris mitigation tool to divert fast ions, which are responsible for erosion effect on collector optic surfaces. The ESA results show the presence of ions ranging from 2 to 13 keV.

Surface roughness of the materials was measured before and after the exposure using AFM, which shows a general increase in roughness of ~2 to 5 times for all materials, with the exception of MLM and Mo–Au samples. In the case of MLM, the Ru capping layer was eroded away, leaving behind the smoother silicon surface. The Mo–Au shows no increase in surface roughness, which is probably because Au might segregate onto the surface along the grain boundaries to refresh the surface removal due to sputtering by ion flux. These results are also confirmed using XRR measurements.

An extensive XRD analysis is presented for all the materials under consideration. SEM was used to analyze the cross sectional film thickness, which shows the erosion ranged from 10 to 50 nm for various materials. We also report ion implantation using XPS and AES for several materials, which are in quantitative agreement with measured ion energies using ESA. A multilayer sample received varying time exposures to the source debris (in steps of 2, 10, 20, and 40M) and the differences in the material properties after were observed. The sample characterization of these time-dependent exposures is performed in great detail. Data from sample analysis and ESA measurements combined indicate ion impact as a mechanism for debris-optics interactions with the possibility of neutral impact also present.

Acknowledgments

The authors would like to thank project manager Ginger Edwards and support from SEMATECH. Additional assistance from Saša Bajt at Lawrence Livermore National Laboratory, Robert Bristol at Intel Components Research, and the Xtreme Technologies GmbH team in Göttingen were appreciated. A portion of this research was carried out

at the Center for Microanalysis of Materials, University of Illinois, which is partially supported by the U.S. Department of Energy under grant DEFG02-91-ER45439.

References

1. V. Bakshi, *EUVL Source Program at International SEMATECH*, EUVL Source Workshop, Santa Clara, CA (2003).
2. J. M. Slaughter, D. W. Schulze, C. R. Hillset al., *J. Appl. Phys.* **76**, 2144 (1994).
3. S. Braun, H. Mai, M. Mosset al., *Jpn. J. Appl. Phys., Part 1* **41**, 4074 (2002).
4. K. C. Thompson, E. Antonsen, M. R. Hendricks, B. E. Jurczyk, M. Williams, and D. N. Ruzic, *Microelectron. Eng.* **83**(3), 476–484 (2006).
5. C. P. Browne, D. S. Craig, and R. M. Williamson, *Rev. Sci. Instrum.* **22**, 952 (1951).
6. J. A. Simpson, *Rev. Sci. Instrum.* **32**, 1283 (1961).
7. F. R. Paolini and G. C. Theodridis, *Rev. Sci. Instrum.* **38**, 579 (1967).
8. E. Antonsen, K. C. Thompson, M. R. Hendricks, D. A. Alman, B. E. Jurczyk, and D. N. Ruzic, *J. Appl. Phys.* **99**(6), 063301 (2006).
9. A. V. Ruban, H. L. Skriver, and J. K. Norskov, *Phys. Rev. B* **59**, 15990 (1999).
10. L. A. Shmaenok, C. C. de Bruijn, H. F. Fledderus, R. Stuik, A. A. Schmidt, D. M. Simanovski, A. V. Sorokin, T. A. Andreeva, and F. Bijkerk, "Demonstration of a foil trap technique to eliminate laser plasma atomicdebris and small particulates," *Proc. SPIE* **3331**, 90–94 (1998).
11. E. L. Antonsen, K. C. Thompson, M. R. Hendricks, D. A. Alman, B. E. Jurczyk, D. N. Ruzic, T. D. Chinh, G. Edwards, S. Wurm, O. Wood, and R. Bristol, "XCEED: XTREME commerial EUV exposure diagnotic experiment," *Proc. SPIE* **5751**, 1192–1202 (2005).
12. B. E. Jurczyk, D. A. Alman, E. L. Antonsen, M. A. Taworski, M. J. Williams, D. N. Ruzic, T. P. Spila, G. Edwards, S. Wurm, C. R. Woods, and R. Bristol, "The effect of debris on collector optics, its mitigation and repair; next-step a gaseous Sn EUV DPP source," *Proc. SPIE* **5751**, 572–577 (2005).
13. S. Bajt, Z. Dai, E. J. Nelson, M. P. Wall, J. Alameda, N. Nguyen, S. Baker, S. C. Robinson, S. S. Taylor, M. Clift, A. Aquila, E. M. Gullkson, and N. V. G. Edwards, "Oxidation resistance of Ru capped EUV multilayers," *Proc. SPIE* **5751**, 118–127 (2005).
14. J. F. Ziegler, J. P. Biersack, and U. Littmark, *The Stopping and Range of Ions in Solids* Pergamon Press, New York (2003).

Biographies and photographs of authors not available.